RESEARCH ARTICLE
Editor's Choice
ADVANCED MATERIALS
www.advmat.de

Mechanical Actuation via Homeomorphic Transformations of Topological Solitons within Polymer Coatings

*Jacques Peixoto, Darian Hall, Dirk J. Broer, Ivan I. Smalyukh, and Danqing Liu**

Topological solitons are currently under investigation for their exotic properties, especially in nonlinear physics, optics, and material sciences. However, challenges of robust generation and limited stability over time have hindered their practical uses. To address this issue, an approach is developed to form structured arrays of solitons in films of polymerizable liquid crystals. Their complex molecular architecture is preserved by in situ photopolymerization forming a stable liquid crystal network. Most excitingly, their properties are advanced to include responsiveness functions. When thermally actuated, these topological solitons mediate the reconfiguration of surface topographies. Complex shape changes occur depending on the intrinsic complex spatial distribution of the director, which may even lead to full shape inversion and topographical changes as high as ≈40% of the initial thickness. Conversely, the shape changes provide information on the initial director profile, which is consistent with the mathematical model. The soliton-containing polymer coatings are applicable in multiple domains, ranging from tunable optics to haptics, and from shape-coupled sensing systems to temperature-coupled heat management.

1. Introduction

Liquid crystals (LCs) are known for their well-controlled molecular organization, which is used to the benefit of liquid crystal displays,[1] diffractive optics,[2] and soft robotic actuators.[3,4] More recently, also relevant for this publication, they enable the development of topographically active polymer surfaces leading to new applications in haptics,[5] robotic fingers,[6] and self-cleaning surfaces.[7] In most cases, long-range order of liquid crystal molecules is guided through external fields or interfacial forces at anisotropic surfaces obtained by rubbing,[8] photoalignment,[9] or surfactants.[10] For most applications, the liquid crystal alignment, as defined by their director n is chosen to be unidirectional, twisted, splayed, or organized around a defect. When chirality is introduced to the liquid crystal, the molecular organization becomes more complex as the director field becomes spatially nonuniform. In its most simple form, describes a continuous twist to form a helix,[11] but more spatially distorted structures are possible as well.[12] In general, the interactions that break the inversion symmetry are weak, and the twisted ground states easily take additional conformations by external fields or surface interactions. For instance, they may lead to particle-like excitations with skyrmion (2D) or toron-shaped (3D) internal director patterns of various complexity.[13,14] They behave as particle-like structures within

J. Peixoto, D. J. Broer, D. Liu
Laboratory of Human Interactive Materials (HIM)
Department of Chemical Engineering and Chemistry
Eindhoven University of Technology
Den Dolech 2, Eindhoven 5612 AZ, The Netherlands
E-mail: d.liu1@tue.nl

J. Peixoto, D. J. Broer, D. Liu
Institute for Complex Molecular Systems (ICMS)
Eindhoven University of Technology
Eindhoven 5600 MB, The Netherlands

D. Hall, I. I. Smalyukh
Department of Physics
University of Colorado
Boulder, CO 80309, USA

I. I. Smalyukh
International Institute for Sustainability with
Knotted Chiral Meta Matter
Hiroshima University
Higashihiroshima 739-0046, Japan

I. I. Smalyukh
Materials Science and Engineering Program
University of Colorado
Boulder, CO 80303, USA

I. I. Smalyukh
Renewable and Sustainable Energy Institute
National Renewable Energy Laboratory and University of Colorado
Boulder, CO 80303, USA

The ORCID identification number(s) for the author(s) of this article can be found under https://doi.org/10.1002/adma.202308425

DOI: 10.1002/adma.202308425

chiral nematic host media and have shown their values for theoretical studies on, for instance, knotted phenomena[15] and advanced optics.[16,17]

2. Results and Discussion

In this study, we convert the complex configurations of chiral liquid crystal order in soliton particles into a solid system of a polymer network with the preservation of the characteristic molecular orientations and structural organization. Not only does this further stabilize the intrinsic molecular organization preventing destabilization of the structure, but it also adds functionalities by inducing thermal surface deformations related to modulations of the orientational order.[18] Director-steered surface deformations have recently been studied for coatings with helicoidal order with fingerprint textures[6] and with singular defects.[19,20] Changing the molecular order by a trigger such as temperature[21] or light,[22] a positive stress builds up orthogonal and a negative stress parallel to the director.[18] The resultant stresses deform the surfaces such that peaks and valleys are being formed, of relevance for surface-active applications including the controls of friction,[23] adhesion,[24] cellular culture,[25] and touch experience.[26] In this paper, we bring the complexity of the director patterns a level higher by introducing polymers with toron-shaped defects that are brought into the coating prior to its polymerization. Various high-level quasiparticles can be photopolymerized as part of a coating or film, such as cholesteric fingers, elementary toron, and twistion. Upon actuation, the complex director patterns within the soliton will lead to evolutions of corresponding complex and unique surface topographies. Conversely, by analyzing the surface deformation, going from a state of high molecular order to a lower ordered state, the initial molecular order can be confirmed, as supported by mathematical modeling.

To form the toron-type solitons, we followed two strategies. First, we adopted the methodology that was published earlier for nonpolymerizable liquid crystals and is based on frustrated alignment confined by two glass substrates together forming a glass cell, and subsequent structure formation by a focused laser beam.[16] Second, we developed a method in which the solitons form spontaneously by applying the coating during an optimized spin coating process. The first method has the advantage that the soliton position can be exactly chosen. The latter simplifies the procedure and is accessible for large areas of coatings by avoiding cell construction. Both methods require a mixture of liquid crystal monomers containing a chiral component. Information on the optimization of the composition concerning chirality and structure formation is provided in Figure S1 (Supporting Information). These mixtures can be processed to a thin film by either filling a cell with a melt of the LC monomers or by spin coating from solution on a single surface-treated glass plate. After the formation of the solitons, the structures are fixed by a photocrosslinking reaction initiated by the small amount of photoinitiator present. From studying free-standing films of liquid crystal networks (LCNs), we know that upon externally driven reduction of the molecular order as defined by scalar order parameter S, either by temperature or by light, anisotropic geometric deformation takes place with an expansion in the directions perpendicular to the director and shrinkage parallel to it.[18] In the case of the confinement of an LCN coating firmly adhered to the substrate it is somewhat more complicated as in the case of director patterns stresses are generated which gives local director-dependent expansion or shrinkage on top of some eventual thermal volume increase.[27] This effect, which in literature is so far studied for more traditional alignment patterns and corresponding length scales, we will utilize here to create complex deformation within the confinement of soliton-like structures.

2.1. Actuation of Torons Formed Under Confined Conditions

In previous studies, it has been shown that topological solitons are generated in a uniform homeotropic background by exposing it locally to a focused laser.[28] The uniform background is imposed by either frustrating the chiral order by strong anchoring alignment layers at both glass substrates or by an electric field unwinding the system.[29] At the location of a tightly focused polarized laser beam, the topological solitons are formed and while being captured by optical tweezers can be spatially distributed in the cell to form a pattern. Subsequently, we photopolymerized the system and, after the removal of the top glass substrate, we obtained a coating populated by a well-defined pattern as is shown in **Figure 1**. For this occasion, we organized the topological particles to form the logo of Eindhoven University. As directly observed from the polarized optical microscope (POM) in Figure 1a, the TU/e logo is readable based on the optical anisotropy of the director pattern in the topological solitons. We analyzed the director pattern by comparing the observed POM images of the solitons with the ones obtained by the numerical modeling of such POMs of a toron (Figure S2, Supporting Information). A toron consists of a torus of double-twisted director twist (Figure 1b) containing two defect points close to the substrate, which matches its complex director structure to the boundary conditions. The spatial distribution of the director n in the x–y plane located at the middle of the cell (Figure 1c) shows a 2D skyrmion-like distribution, where a π rotation is occurring from the center to the edge. A more complex distribution is depicted in the y–z plane (Figure 1d), where the middle of the toron shows a vectorized director field $\boldsymbol{n}(\boldsymbol{r})$ distribution from top to bottom corresponding to the formation of the two opposite ± 1 point defects represented by two red spheres in Figure 1b,d. Under the POM, they are distinguishable by their circular shape, and their distribution of the edge brightness related to the orientations of the crossed polarizers while the middle part remains dark due to the homeotropic orientation of the molecules (Figure 1f). This behavior is also observable in the corresponding computer-simulated POM image (Figure 1e), which closely matches the experimental counterpart (Figure 1f).

Surprisingly, after the preparation of the film and removal of the top glass plate, the white light interferometry (WLI) analysis revealed that the torons mediate the formation of the little indents observed on the surface at room temperature (Figure 1i). The circularly shaped indents have a diameter comparable to the pitch. These indents can be explained by taking both the polymerization temperature of 45 °C and the director pattern of the topological soliton into account. At the polymerization temperature, the film is, apart from minor polymerization shrinkage, in tensionless conditions as in the liquid prior to polymerization. Upon cooling to room temperature, the order parameter increases

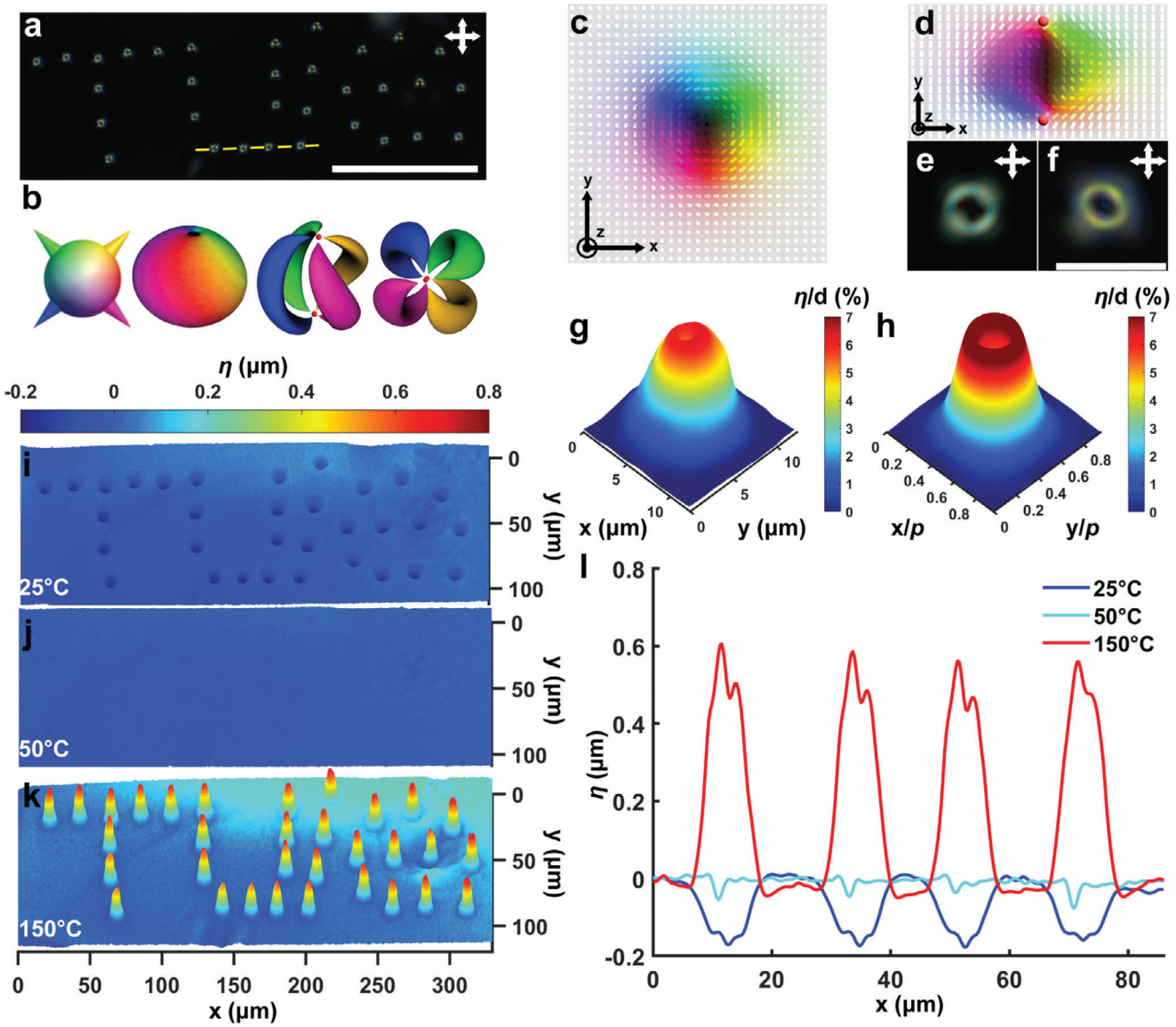

Figure 1. Polymerized homeotropic liquid crystal with embedded torons. a) Polarizing optical microscope (POM) image of the homeotropic chiral liquid crystal polymer network with a pattern of torons created by laser beam's writing and steering prior to its polymerization. The scale bar represents 100 μm. b) Visualization of the director fields. The vectors decorating the nonpolar $\boldsymbol{n}(c)$ via smooth vectorization are colored based on their orientations as shown in the order-parameter space (left), preimages (Section S2, Supporting Information) of vector orientation for all the directions (mid-left), for four orientations and a view at 45° (mid-right) and top view (right) with the vector colors matching the cones of the upper right figure. c,d) Director field within a toron in the c) x–y and d) y–z planes in the center of the structure. The color scheme depicting orientations is based on panel (b), red spheres corresponding to the point defects. e) Numerical POM image using Nemaktis software (Section S2, Supporting Information) of a toron based on $p = 10.5$ μm, $d = 10$ μm, extraordinary and ordinary refractive indices $n_e = 1.60$, $n_o = 1.53$. f) POM image of an isolated toron from panel (a). Scale bar represents 10 μm. g) Surface topography of a single toron at 150 °C. h) Simulated topographic deformation of a single toron at 150 °C based on a voxel model combined with the equilibrium director field modeling (Section S2, Supporting Information). i–k) Surface topography measured by white interferometry at i) 25 °C, j) 50 °C, and k) 150 °C. l) Topographical profiles of four neighboring torons depicted by the yellow dashed lines (panel (a)) at different temperatures.

leading to shrinkage-related stresses of the in-plane-oriented director area with respect to the normal, and expansion-related stress occurs in homeotropic areas with the director orthogonal to surfaces. With the removal of the top glass plate, the stresses relax by the formation of the indents. When heating again to temperatures close to the polymerization temperature, the order parameter takes its initial value as it had during and after polymerization. This can be also concluded from Figure 1j taken at 50 °C which reveals a flat surface again.

A further increase in temperature prompts the formation of the protrusion with volcano-shaped tips, exactly as one would expect from the director distribution within the toron. The WLI image in Figure 1k now shows a protrusion at the initial location of the indent. In the center of the toron, the homeotropic

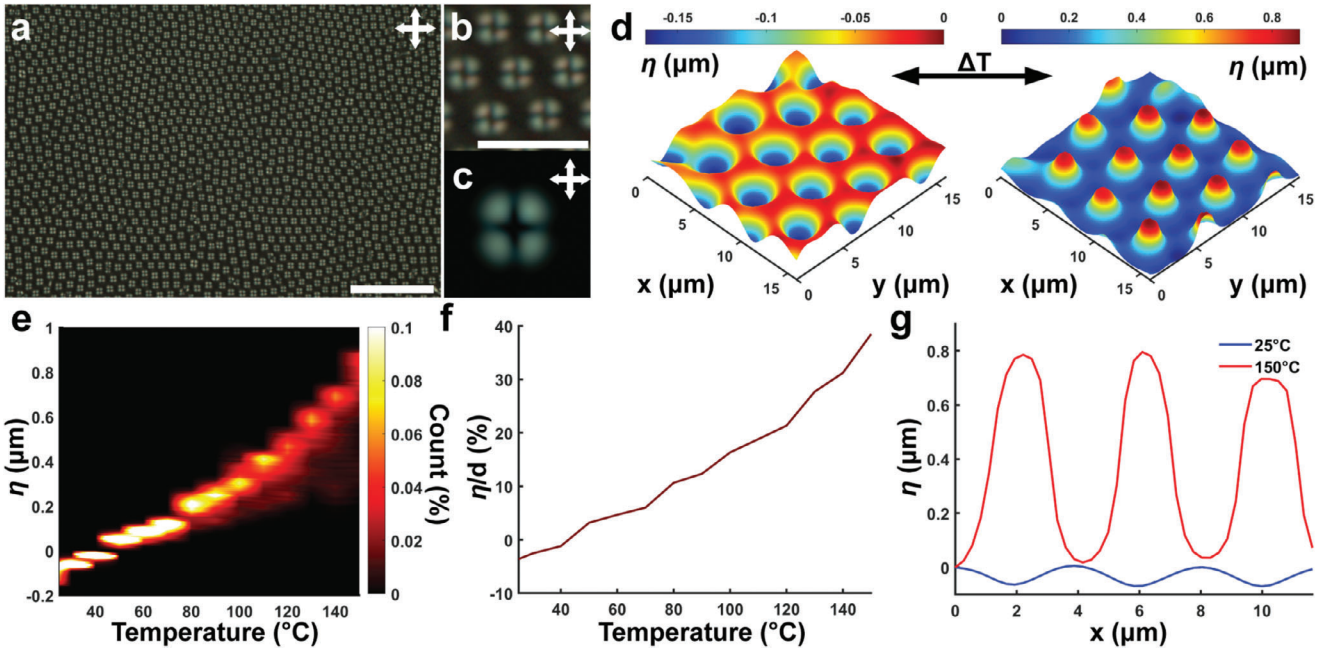

Figure 2. Surface properties of self-assembled torons in a thin coating. a–c) POM image of a large area of torons after polymerization, a) with the directions of the crossed polarizers shown in the inset and with the scale bar being 25 μm, b) zoomed view to show the Wigner crystal-like hexagonal lattice, scale bar is 4 μm, and c) simulated image (obtained using Nematkis software) of a toron for parameters, $p = 2.5$ μm, $d = 2$ μm, $n_o = 1.53$, and $n_e = 1.60$. d) 3D map obtained using white light interferometry at 25 and 150 °C. e) Statistical height distribution as a function of temperature with steps of 10 °C based on histograms with a bin size of 0.01 μm and a sample size of ≈5000. f) Relative height as a function of temperature from the biggest population of torons normalized by the initial film thickness of 2.1 μm. g) Profiles were taken along centers of three linearly aligned torons at 25 and 150 °C.

alignment gives shrinkage in comparison to its azimuthally planar surrounding which is committed to expansion. So, interestingly, if one would call the surface profile at low temperatures the negative 3D topographic image of the toron, they deform in a homotopic way to a positive image at higher temperatures. A relative height $\eta(t) = h(t) - d_0$ (with $h(t)$ being the absolute height at a specific temperature and d_0 the thickness at 25 °C) of ≈580 nm is obtained at 150 °C (Figure 1k,l). It leads to an increase of the reversible out-of-plane modulation to 7.5% of the initial coating thickness. The experimental observation agrees with the model (Figure 1g,h). In our model, we take the corresponding structure calculated by minimizing the Frank–Oseen free energy and assign each voxel an effective height function that we fit empirically to our data. Besides the formation of a deep indent explained by the presence of a small homeotropic region in the middle of the toron, a larger height contraction is expected by the model. The experiments reveal a smaller indent as being limited by the resolution of our measurement. Temporal and thermal stability was investigated, showing long-term stability (>1 year) and reproducibility over multiple cycles with minor fluctuations (Section S7, Supporting Information).

2.2. Thin-Film Self-Assembly of Torons and Their Thermal Actuation

Although the above-described cell method in combination with laser tweezer steering has the advantage of exact placement of the soliton particles, it might be less suitable for scaling it up to larger areas. Therefore, we investigated whether spontaneous formation of the solitonic particles is possible in our reactive liquid crystal mixture based on self-assembly in spin-coated films. By fine-tuning the ratio d/p, torons and cholesteric fingers can be spontaneously generated. An example of finger formation is shown in Figure S3 (Supporting Information). For a ratio of $d/p \approx 0.8$ ($d \approx 2.1$ μm and $p = 2.5$ μm), large areas (≈mm^2) with Wigner crystal-like hexagonal lattice of topological solitons are observed (**Figure 2a,b**), which is intrinsic for self-assembly processes of repulsively interacting pseudoparticles in 2D lattices.[30] Here, the ratio d/p needs to be lower than for the cell configuration as the air interface provides weaker homeotropic anchoring than the polyimide at the glass cell surface. The corresponding POM image (Figure 2b) is close to the computer-simulated one (Figure 2c). The difference aspect with the previous one (Figure 1e,f) comes from the change in optical retardation caused by the thickness difference. The black crosses in the images correspond to the crossed polarizers' orientation and show the area where the projected molecular orientation within the toron is roughly parallel to one of the polarizers. The colored parabolic birefringence fields confirm the molecular alignment within the toron, as also affirmed by the comparison with the modeled POM pattern in Figure 2c.

At room temperature, the surface is pseudoflat and populated by indents of ≈80 nm deep and a diameter equal to the pitch of the molecular helix (Figure 2d, left). The explanation of the formation of the indents is similar as they form upon cooling from the polymerization temperature to room temperature. Upon heating, the inversion from indent to protrusion

occurs corresponding to homeomorphic actuation of the topological soliton around the temperature at which the film was polymerized (Figure 2f,g). By raising the temperature further, protrusions form with a height of ≈800 nm at 150 °C (Figure 2d, right). Unlike the previous case, the protrusions do not show an obvious volcano tip. The resolution of our topographical analysis limits an exact graphical representation of somewhat smaller-sized torons. Moreover, the homeotropic area located in the middle of the toron is rather small, which also sets mechanical limits to the indent formation at the top of a relatively high protrusion.

Since the system is based on self-assembly, a statistical analysis of the height distribution as the function of temperature has been performed with a sample size of ≈5000 elements (Figure 2e). We notice a broadening of the distribution as the temperature increases. This is attributed to the presence of defects in the coating and small changes in the homeotropic surrounding of an individual toron, which exercises a positive stress on the toron's planar area as temperature increases. The environment of the toron is an important variable of the maximum height of the protrusion, as shown in previous studies for different patterns.[31] To support this argument, we study the dependencies of the height as a function of the density of its location. The result shows a dependency and an optimum density of ≈0.06–0.08 toron μm^{-2} (Figure S4, Supporting Information).

2.3. Generation of 3D-Localized Topological Solitons with Higher Complexity

So far, we investigated the simplest topological solitons that form in our coatings. However, under the right conditions, the coatings are very rich in the formation of more complex solitons as well. For this study, we selected a twistion and a highly twisted toron. A twistion can be seen as the fusion of two torons[32] spontaneously embedded into our material prior to its polymerization when $d/p \lessapprox 1$ (**Figure 3a**). The net total topological charge of the structure is embedded in the uniform far field background. It contains six self-compensating hyperbolic defects (Figure 3b–f). Each toron has two defects, as well as possesses a small area twisting in a direction opposite to the one induced by the medium's intrinsic chirality, localized around two point defects at the middle part (Figure 3d).[27] It can be viewed as a stretched double-twist torus and is easily distinguishable from the POM and computer-simulated version by its bowtie shape (Figure 3g,h). Structurally, a twistion has unique features determined by the coupling between the two torons and the localization of the defect points.[32] From the surface topography standpoint, at room temperature, it forms two ≈200 nm connected holes of ≈15 µm diameter (Figure 3k). The inversion still occurs; however, at 50 °C the surface is not flat; instead a remaining S-shaped valley is observed (Figure 3l). At 150 °C (Figure 3m) the inverted complex surface topography is formed. It shows an eight shape composed of two half donuts with a height of 1 µm and surrounded by a crown ridge of ≈0.5 µm height and is somewhat more complex than the numerically modeled structure provided in Figure 3i. The richness of the structure comes from the complex spatial distribution of the director . In that case, it differs largely from the top to the bottom, induced by the twist inversion and the asymmetry formed by the defect points along the *z*-axis. The numerical model closely predicts the overall shape but struggles to catch the fine details of the separation that occurs in the center of the structure, which is partially due to the adopted approximations neglecting the changes around the defect points in combination with the complex changes in the area containing the twist inversion. A profile has been collected parallel to the long axes, as depicted in Figure 3h, and the corresponding result for different temperatures is shown in Figure 3j. In this condition, a complex reversible surface modulation has been achieved which is coupled to a maximum out-of-plane modulation of ≈12%. Corresponding observations of the thermal morphing of the various topological soliton structures are given in Figure S5 (Supporting Information).

Complex solitonic structures, featuring more than π-twist from center to periphery,[29] have been obtained by fine-tuning the ratio $d/p \approx 0.65$ (**Figure 4a**). From the simulated POM image (Figure S6e, Supporting Information), we anticipate this structure to be a cholesteric finger of type 1 looped on itself,[24] so that POM reveals a characteristic pattern with three bright regions that are reproduced in numerical modeling of the POM image. Details of the corresponding solitonic director field configuration are revealed in Figure S6 (Supporting Information). The overall lateral size of this solitonic structure is close to 15 µm (Figure 4a,b). The surface topography displays circular symmetry. At room temperature, a hole of ≈180 nm deep is formed with a bump in the middle. Also, this structure is inverting its surface topography at elevated temperatures, in this case at ≈60 °C (Figure 4e). Then, at even higher temperatures, the behavior is different from that seen in the previous examples discussed above. The central part relaxes to the bottom while the rest of the structure elevates to form a volcano shape of ≈10 µm diameter at 150 °C (Figure 4f), a circular wall in the topography of ≈350 nm height, and a depression deepness of ≈150 nm (Figure 4g,h). Interestingly, also this structure reveals surface topography/shape as predicted by the model (Figure 4c,d,f). We anticipate that the region with planar alignment is considerably bigger in comparison to the other defects, thereby mitigating the stresses from the outer and inner homeotropic regions. The complex actuation mechanism of this structure shows the wave-like torsion propagating along the coating induced by the frustration exerted by the rigid substrate.

While our findings described above reveal actuation of surface topography with the help of solitonic structures of director field, which are localized in all three spatial dimensions and yield thin-film surface topography actuations in regions with the lateral extent comparable to cholesteric pitch, Section S3 (Supporting Information) shows how similar effects can be achieved for translationally invariant solitonic structures of domain walls and cholesteric fingers of different types.

3. Conclusion and Outlook

We have demonstrated the potential of topological solitons as good candidates for shaping the modulation of the surface topography in thin polymeric coatings. For this purpose, we formulated a composition that allows us to embed and freeze them without losing their complex spatial distribution of molecular alignment. Two strategies have been developed: a laser-controlled method to write a spatially controlled pattern of the solitons,

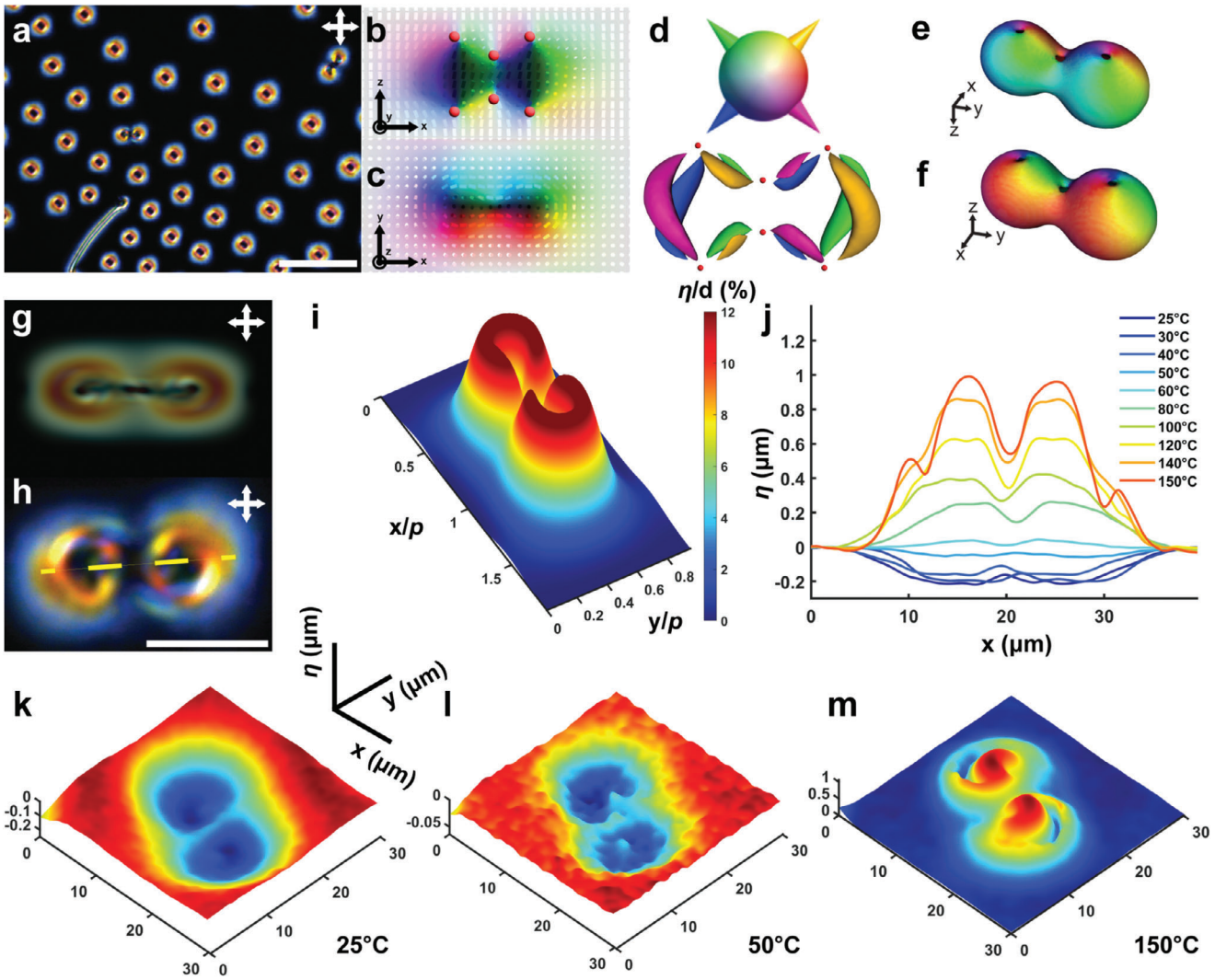

Figure 3. Actuation of spontaneously formed twistions. a) POM of a polymerized coating after frustration induced by isotropic to cholesteric phase transition during their monomeric state, showing twistions, torons, and a cholesteric finger, directions of the crossed polarizers depicted in the inset, the scale bar is 60 μm. b,c) Director field within a toron in b) *x*–*z* and c) *x*–*y*. The color scheme is based on panel (d). d–f) Visualization of the director fields. The colors indicate the orientation of the smoothly vectorized director: d) side views of four orientations, e) bottom side, and f) top side. g) Numerical POM image using Nematkis of a twistion based on $p = 10$ μm, $d = 10$ μm, $n_e = 1.60$, and $n_o = 1.53$. h) Corresponding observed POM image, the scale bar is 10 μm. i) Numerically predicted deformation of the twistion at 150 °C based on a voxel model (see Section S2 in the Supporting Information). j) Profiles of a twistion at different temperatures. The sampling location is depicted by the yellow dashed line in panel (h). k–m) Surface topography measured by white interferometry at k) 25 °C, l) 50 °C, and m) 150 °C.

and a self-assembling approach suitable for higher resolution in a simpler scalable manner as compared to conventional lithographic processes. We studied five different structures including torons, twistions, cholesteric fingers (types 1 and 3), and axisymmetric twisted solitonic structures that are loops of cholesteric fingers of the first type. Their complex topologically distinct configurations are directly translated into exotic reversible surface modulation upon thermal actuation. The surface topography changes from spherical valleys to protrusion by passing through an intermediate flat state close to the temperature at which they were photopolymerized. When combined with the controlled spatial distribution we obtain erasable predesigned topography patterns. The maximum deformation achieved is 40% with respect to the initial thickness, which is more than three times larger than previously reported for chiral fingerprint textures.[11]

The numerical height model utilized in this work coarse grains the complex stresses that build in the polymer coatings leading to an effective actuation dependent on the director orientation along the *z*-axis. In exchange for acquiring this effective height function, the *xy* spatial degrees of freedom were removed from the model. Therefore, we envision that the model can be generalized by retaining the global stresses generated in the modeled coating while the film is fixed to the substrate.

For future work, the properties of each soliton such as birefringence and modulation could be fine-tuned in relation to the desired applications. Besides the topological objects studied in this work, solitonic and singular structures representing other

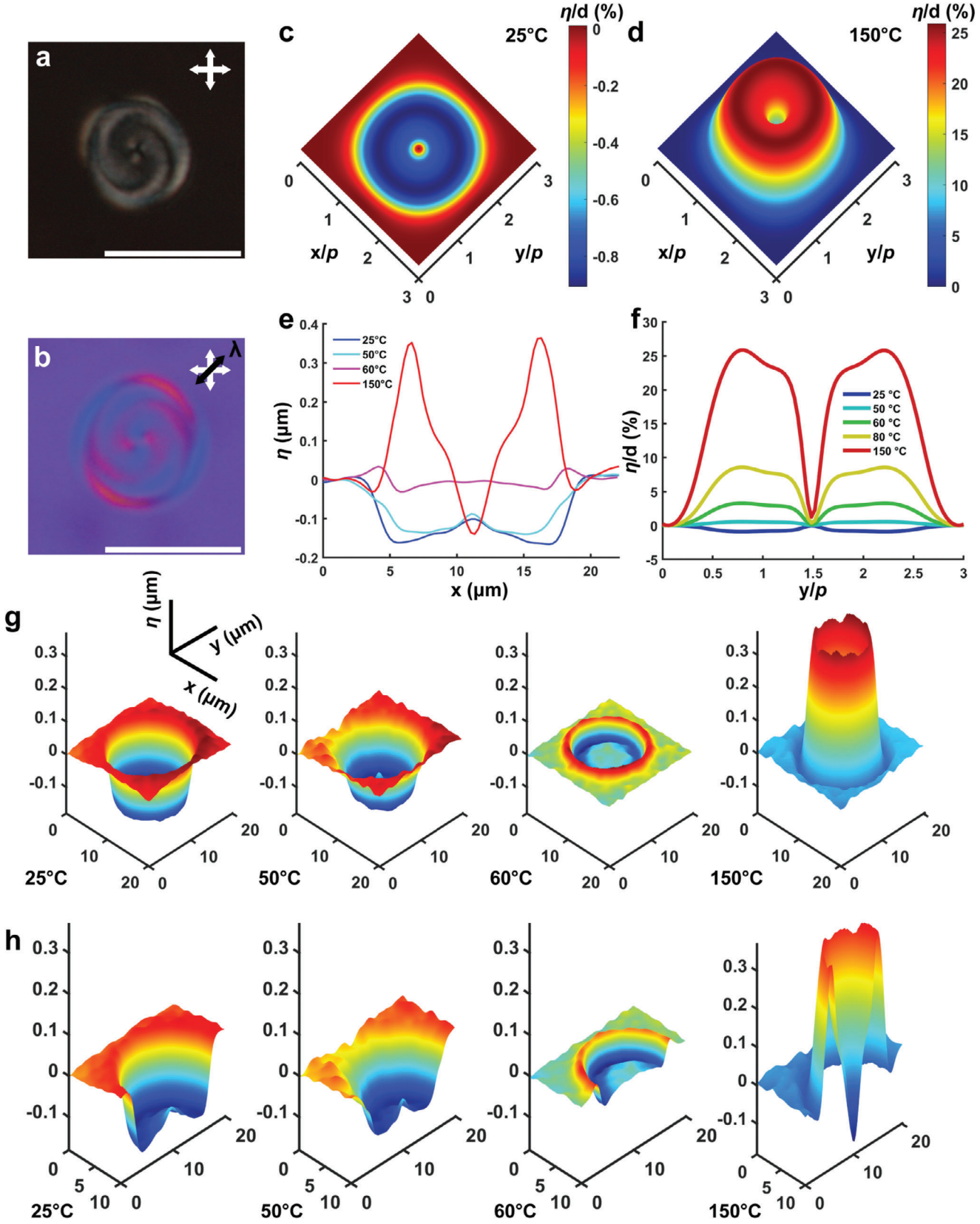

Figure 4. Axisymmetric twisted soliton. a) POM of a photopolymerized complex defect with crossed polarizers. b) Numerical POM image computer-simulated using Nemaktis software for a looped cholesteric finger of the first type (CF1), shown in Figure S6 (Supporting Information), based on p =

homotopy groups[33] can be hosted to broaden the library of polymer-embedded topological configurations and their utility. Further investigation of different stimuli such as light, electricity, and chemical environment can be explored to extend the range of applications. We anticipate that the demonstrated stabilization of topological solitons, their complex responsiveness to external stimuli, optical anisotropy, and exotic distribution of the director n will make the polymer coatings suitable for applications in various tunable optical devices,[34] dynamic surface topographies for tribology, wettability,[35] haptics,[36] chemical traps, and sensors.[37]

4. Experimental Section

Materials: A mixture was used based on six different components described in Figures S1 (Supporting Information): **1**–**3** were monomers and obtained from Merck UK; **4** was a monomer with an asymmetric carbon and was obtained from BASF; **5** was an azobenzene-type monomer and custom-synthesized by Syncom (Groningen, Netherlands); **6** was a photoinitiator obtained from BASF (Irgacure 819). The proportion of each compound is summarized in Figure S1 (Supporting Information).

Substrate Preparation: The glass substrates were cleaned by two sonification baths: first with acetone, followed by propanol-2 for 20 min each. The surface was activated by ozone exposure (UV–ozone photoreactor PR-100) for 20 min. The glass slides were spin-coated (using a commercial instrument Laurell WS-650-23) with a polyimide layer inducing homeotropic alignment (SE5661 Nissan SUNEVER) (STEP1: 800/5/500 STEP2: 5000 rpm /40 s/800 rpm. s^{-1}). Subsequently, they were prebaked at 90 °C for 10 min and baked at 190 °C for 90 min.

Cell Preparation and Laser Tweezers: The mixture was diluted and mixed into tetrahydrofuran to ensure the homogeneity of the different components. After evaporation of the solvent overnight, the mixture was filled into cells formed by two indium tin oxide (ITO) glass slides pretreated with SE5661. The thickness of the cell was fixed by 10 µm silica spacers combined with UV glue. Torons were created by using laser tweezers with a power of 100 mW, as described in refs. [11,12,21]. After generation, the torons were optically manipulated with the laser tweezers at a lower power of the order of 10 mW, remaining stable when spatially translated. The utilized laser tweezer setup was built around an inverted optical microscope (IX-81, Olympus) and also comprised a 1064 nm ytterbium-doped fiber laser (YLR-10-1064, IPG Photonics) and a phase-only spatial light modulator (P512-1064, Boulder Nonlinear Systems), in addition to various lenses and other optical elements described in detail elsewhere.[11,12,21] In some cells, torons were further controlled by applying a 1 kHz AC sinusoidal voltage across the gap between ITO glass substrates using a function generator (DS345, Standford Research Systems).

The Dynamic Spin Coating Process: The monomer mixture was diluted in tetrahydrofuran with a solid concentration of 32% and mixed using a steering magnet. 200 µL of the solution was deposited in the middle of the glass when the maximum speed was reached. The used settings were 1500 rpm/35 s/100 rpm s^{-1}.

Polymerization: Photopolymerization of spin-coated films was achieved by exposure to a 200 W mercury lamp filtered by a short-pass (<400 nm) filter to avoid the activation of the azobenzene in a nitrogen environment and at 45 °C (chiral nematic phase) for 5 min with a light intensity ≈15 mW cm^{-2} controlled by an Ominicure series 2000 light source.

Photopolymerization in cells was done in situ with a homebuilt setup on the stage of an Olympus IX-81 microscope using a 20 W mercury bulb filtered by a 435/20 nm line filter and a photomask cutting off all other UV light aside from a small pinhole of ≈100 µm. The corresponding light intensity that reached the sample after diverging from the pinhole to the sample was estimated to be ≈30 mW cm^{-2}.

Surface Characterization and Actuation: The thickness of the coating and surface modulation were recorded using white light interferometry (Sensofar Neox) coupled to a hotplate (Linkam TMS 94). Topological soliton recognition, analysis, and localization were done by using a polarized optical microscope (Leica DM6000M). To ensure full relaxation of the coating at the desired temperature, it was waited for at least 30 s before any acquisition.

Statistical Analysis: The statistical analysis of the self-assembled toron was done using a homemade script based on the imregionalmax function of Matlab software.

Director Structure Simulation: All relaxed structures of the chiral nematic before polymerization were modeled by numerically minimizing the Frank–Oseen free energy to an equilibrium state on a discretized 3D grid. In the model, the known properties of 4-Cyano-4'-pentylbiphenyl were implemented representing the mixture. This was validated as the material is mostly composed of molecules of similar size and polarity with monoacrylate (>75%), including 30% of a liquid crystal functionalized with a cyano group. Further information on modeling is available in the Supporting Information.

POM Simulation: Each POM was computed via the software Nemaktis by importing the corresponding relaxed structure, cell dimensions, and refractive indices. The refractive indices used for the simulated POM images were measured previously in a similar system.[38]

Modeling: The surface topography was obtained from each relaxed structure by assigning an effective height function to each column-oriented along the *z*-axis and summing over the effective heights to compute the overall topography. See the Supporting Information for more details.

Supporting Information

Supporting Information is available from the Wiley Online Library or from the author.

Acknowledgements

This research formed part of the research program financed by the Dutch Research Council (NWO) (OCENW.KLEIN. 10854, START-UP 8872, and Gravity Program 024.005.020—Interactive Polymer Materials IPM). The authors thank A. Repula for technical assistance. D.H. and I.I.S. acknowledge the hospitality and support of the Institute for Complex Molecular Systems at the Technical University of Eindhoven during their collaborative visit, where they were working toward the goals of this article. Research at CU-Boulder (D.H. and I.I.S.) was supported by the US Department of Energy, Office of Basic Energy Sciences, Division of Materials Sciences and Engineering, under contract DE-SC0019293 with the University of Colorado at Boulder.

Conflict of Interest

The authors declare no conflict of interest.

Author Contributions

J. P. and D. H. contributed equally to this work. J.P. performed the experiments and analyzed data. D.H. conducted modeling and interpreted the

2.5 µm, $d = 2$ µm, $n_e = 1.60$, and $n_o = 1.53$. POM obtained with a 530 nm retardation plate depicted with a black double arrow. c,d) Numerically predicted deformation of the CF1 loop at c) 25 °C and d) 150 °C based on a voxel model (see Section S2 in the Supporting Information). The scale bar represents 15 µm. e,f) Surface topography profiles of e) the structure at different temperatures and f) the corresponding simulated profile based on Section S2 (Supporting Information). g) Surface topography measured by white interferometry at 25, 50, 60, and 150 °C, and h) the corresponding profiles shown while being intersected at the center of the structure.

results. D.J.B., I.I.S., and D.L. conceived and designed the project. All authors contributed to the writing.

Data Availability Statement

The data that support the findings of this study are available from the corresponding author upon reasonable request.

Keywords

liquid crystal polymer networks, numerical modeling, reversible surface topographies, self-assembly, topological defects

Received: August 19, 2023
Revised: November 11, 2023
Published online: November 23, 2023

[1] H. Kawamoto, *Proc. IEEE* **2002**, *90*, 460.
[2] A. Ryabchun, A. Bobrovsky, *Adv. Opt. Mater.* **2018**, *6*, 1800335.
[3] M. López-Valdeolivas, D. Liu, D. J. Broer, C. Sánchez-Somolinos, *Macromol. Rapid Commun.* **2018**, *39*, 1700710.
[4] C. Zhu, Y. Lu, L. Jiang, Y. Yu, *Adv. Funct. Mater.* **2021**, *31*, 2009835.
[5] J. Gao, Y. He, X. Cong, H. Yi, J. Guo, *ACS Appl. Mater. Interfaces* **2022**, *14*, 53348.
[6] D. Liu, D. J. Broer, *Angew. Chem., Int. Ed.* **2014**, *53*, 4542.
[7] W. Feng, D. J. Broer, D. Liu, *Adv. Mater.* **2018**, *30*, 1704970.
[8] J.-S. Yu, J. H. Lee, J.-Y. Lee, J.-H. Kim, *Soft Matter* **2023**, *19*, 2446.
[9] V. Kumar, Z. Ye, H. Jiang, Y. Shi, K. Li, D. Gérard, D. Luo, Q. Mu, Y. J. Liu, *ACS Appl. Electron. Mater.* **2020**, *2*, 2017.
[10] J. M. Brake, A. D. Mezera, N. L. Abbott, *Langmuir* **2003**, *19*, 6436.
[11] D. Liu, C. W. M. Bastiaansen, J. M. J. den Toonder, D. J. Broer, *Macromolecules* **2012**, *45*, 8005.
[12] G. Cordoyiannis, M. Lavrič, V. Tzitzios, M. Trček, I. Lelidis, G. Nounesis, S. Kralj, J. Thoen, Z. Kutnjak, *Nanomaterials* **2021**, *11*, 2968.
[13] J.-S. B. Tai, I. I. Smalyukh, *Phys. Rev. E: Stat., Nonlinear, Soft Matter Phys.* **2020**, *101*, 042702.
[14] I. I. Smalyukh, Y. Lansac, N. A. Clark, R. P. Trivedi, *Nat. Mater.* **2010**, *9*, 139.
[15] T. Machon, G. P. Alexander, *Phys. Rev. Lett.* **2014**, *113*, 027801.
[16] P. J. Ackerman, Z. Qi, I. I. Smalyukh, *Phys. Rev. E: Stat., Nonlinear, Soft Matter Phys.* **2012**, *86*, 021703.
[17] G. Poy, A. J. Hess, A. J. Seracuse, M. Paul, S. Žumer, I. I. Smalyukh, *Nat. Photonics* **2022**, *16*, 454.
[18] M. Warner, E. Terentjev, *Liquid Crystal Elastomers*, Oxford University Press, Oxford **2003**.
[19] G. Babakhanova, T. Turiv, Y. Guo, M. Hendrikx, Q.-H. Wei, A. P. H. J. Schenning, D. J. Broer, O. D. Lavrentovich, *Nat. Commun.* **2018**, *9*, 456.
[20] T. J. White, D. J. Broer, *Nat. Mater.* **2015**, *14*, 1087.
[21] T. H. Ware, M. E. McConney, J. J. Wie, V. P. Tondiglia, T. J. White, *Science* **2015**, *347*, 982.
[22] K. Mehta, A. R. Peeketi, L. Liu, D. Broer, P. Onck, R. K. Annabattula, *Appl. Phys. Rev.* **2020**, *7*, 041306.
[23] D. Liu, D. J. Broer, *Soft Matter* **2014**, *10*, 7952.
[24] W. Feng, L. Chu, M. B. de Rooij, D. Liu, D. J. Broer, *Adv. Sci.* **2021**, *8*, 2004051.
[25] C. Fedele, E. Mäntylä, B. Belardi, T. Hamkins-Indik, S. Cavalli, P. A. Netti, D. A. Fletcher, S. Nymark, A. Priimagi, T. O. Ihalainen, *Sci. Rep.* **2020**, *10*, 15329.
[26] I. Kurylo, J. van der Tol, N. Colonnese, D. J. Broer, D. Liu, *Sci. Rep.* **2022**, *12*, 19512.
[27] F. L. L. Visschers, M. Hendrikx, Y. Zhan, D. Liu, *Soft Matter* **2018**, *14*, 4898.
[28] I. I. Smalyukh, D. Kaputa, A. V. Kachynski, A. N. Kuzmin, P. J. Ackerman, C. W. Twombly, T. Lee, R. P. Trivedi, P. N. Prasad, *Opt. Express* **2012**, *20*, 6870.
[29] I. I. Smalyukh, B. I. Senyuk, P. Palffy-Muhoray, O. D. Lavrentovich, H. Huang, E. C. Gartland, V. H. Bodnar, T. Kosa, B. Taheri, *Phys. Rev. E: Stat., Nonlinear, Soft Matter Phys.* **2005**, *72*, 061707.
[30] G. Soligno, M. Dijkstra, R. van Roij, *Phys. Rev. Lett.* **2016**, *116*, 258001.
[31] R. You, S. Kang, C. Lee, J. Jeon, J. J. Wie, T.-S. Kim, D. K. Yoon, *ACS Appl. Mater. Interfaces* **2021**, *13*, 36253.
[32] P. J. Ackerman, I. I. Smalyukh, *Phys. Rev. E* **2016**, *93*, 052702.
[33] J.-S. Wu, I. I. Smalyukh, *Liq. Cryst. Rev.* **2022**, *0*, 1.
[34] A. Varanytsia, G. Posnjak, U. Mur, V. Joshi, K. Darrah, I. Muševič, S. Čopar, L.-C. Chien, *Sci. Rep.* **2017**, *7*, 16149.
[35] S. S. Latthe, C. Terashima, K. Nakata, A. Fujishima, *Molecules* **2014**, *19*, 4256.
[36] A. Ryabchun, F. Lancia, N. Katsonis, *ACS Appl. Mater. Interfaces* **2021**, *13*, 4777.
[37] R. J. Carlton, J. T. Hunter, D. S. Miller, R. Abbasi, P. C. Mushenheim, L. N. Tan, N. L. Abbott, *Liq. Cryst. Rev.* **2013**, *1*, 29.
[38] D. J. Broer, R. A. M. Hikmet, G. Challa, *Die Makromol. Chem.* **1989**, *190*, 3201.